Engineering Transactions, **73**(4): 555–578, 2025, https://doi.org/10.24423/engtrans.3546.2025
Institute of Fundamental Technological Research Polish Academy of Sciences (IPPT PAN)
Université de Lorraine • Poznan University of Technology

Research Paper

Multi-Objective Design of a Pneumatic Adaptive Impact Absorber

Rafał WISZOWATY*, Cezary GRACZYKOWSKI, Grzegorz MIKUŁOWSKI, Jan HOLNICKI-SZULC, Zbigniew WOŁEJSZA, Anita ORŁOWSKA-GAŁĘZIA, Łukasz JANKOWSKI

Institute of Fundamental Technological Research, Polish Academy of Sciences
Warsaw, Poland

*Corresponding Author e-mail: rwisz@ippt.pan.pl

This manuscript proposes a multicriteria approach to the design optimization of adaptive pneumatic impact absorbers. The considered absorber consists of two sealed chambers separated by a piston with an internal valve. Proper valve control affects gas flow between the chambers and ensures a flat reaction force profile over a possibly long piston stroke. The design of such an absorber is defined by three parameters: initial gas pressure, diameter, and length. For a given range of impact conditions, the worst-case maximum deceleration and maximum mass flow rate are used as design criteria in a multicriterial minimization problem. Solutions to this problem provide an optimal balance between impact absorption performance and the technical requirements the valve must meet. An example is considered, which illustrates the Pareto-optimal solutions in the design space and the complex interdependency between initial pressure and absorber diameter at each absorber length. The results demonstrate that a proper choice of design parameters can result in significant performance improvements.

Keywords: adaptive pneumatic absorbers; impact absorption; design optimization; multi-objective optimization; mass flow rate.

1. Introduction

One of the fundamental issues encountered in engineering practice is the dissipation of impact energy [1]. Many devices, as well as transported or sorted objects, are exposed to short-duration harmful mechanical loads. This problem is particularly relevant to the functioning of production lines [2] and aircraft landing gears [3]. Various energy dissipation and harvesting systems [4] are used to reduce the stresses resulting from such loads. These include friction elements, elastic or elasto-plastic components, gas-filled enclosures (such as vehicle airbags or

drop-cushioning airbags) [5], and cylinder impact energy absorbers consisting of a sleeve and a piston [6]. The working medium used in the latter type of absorbers is often a gas (that imparts elastic properties to the absorber) or a liquid combined with gas (that provide, respectively, damping characteristics and elastic compliance). This distinction results in the following basic classification of absorbers that utilize fluid as an energy dissipation medium [7]:

1) gas/pneumatic absorbers (buffer/stop cylinders, various pneumatic devices [8]),
2) oil absorbers, in which oil is displaced by the piston as it moves within the cylinder sleeve [9–11]. The oil acts as a damping medium for the movement of the piston and piston rod, but its low compressibility may limit the elastic properties of the absorber,
3) hydropneumatic absorbers that combine both oil and gas. The oil serves as the damping medium for piston movement, while the absorber's compliance is primarily determined by the gas in the cylinder [12].

An important advantage of pneumatic absorbers is that they can be designed as devices that do not require petroleum-based substances. This may be particularly desirable in applications within the food industry [13, 14] and in other manufacturing sectors where cleanliness control is essential [15, 16]. A disadvantage of pneumatic absorbers is that their passive implementations exhibit considerably lower efficiency than passive hydropneumatic absorbers, where the efficiency of the latter ones ranges from 80% to 90% [7, 17].

Impact-absorbing devices can be further classified based on the absence or presence, and the type of impact process control [18]:

– passive systems, which are not able to adapt their mechanical characteristics to specific impact characteristics [19, 20],
– semi-active systems, which, in response to varying impact conditions, can be controlled to minimize the impact force without requiring the supply of external energy that would need to be accounted for in the impact absorption model [21]. Typically, a controllable valve is used as the actuator,
– active systems, which are similar to semi-active systems, with the key difference that the external energy supplied to the system plays a significant role in the impact energy balance [22, 23]. A typical implementation may involve a pump and an external gas supply or storage tank.

The primary advantage of passive absorbers is their structural simplicity, which contributes to their reliability. However, in practical applications, impact absorbers are required to minimize the impact force across a wide range of impact energies and initial velocities of the impacting object. These objectives can be formalized as:

– achieving a nearly constant reaction force from the absorber while utilizing the entire available braking distance,
– ensuring a wide range of impact velocities and energies for which the absorber exhibits such a constant reaction force response.

It is difficult to achieve these objectives purely through passive means, which stimulates research in active and semi-active systems.

The literature includes many ingenious and practical models and control methods dedicated to semi-active impact absorbers. A comprehensive review of magnetorheological absorbers and their formal models can be found in [24]. A specific semi-active solution designed for landing gears and based on convolutional neural networks is described in [25], while [26] proposes two types of semi-active controllers: a model predictive controller and a neural controller based on reinforcement learning. Reference [27] presents an extensive discussion and overview of various pneumatic absorbers, along with their mathematical models. A control method for a pneumatic shock absorber under unknown impact conditions is proposed and experimentally validated in [28]. In [29, 30], two methods based on the model predictive control approach are introduced, enabling efficient realization of impact absorption process without prior knowledge of selected system and excitation parameters. Finally, the optimization of a semi-actively controlled pneumatic rescue cushion is analyzed in [31].

However, most existing research in this field focuses on the control methods and response analysis of the employed semi-active absorbers, while their design parameters are often assumed ad hoc or adopted from manufacturers' data. In contrast, this paper considers a specific semi-active pneumatic absorber and addresses the problem of its optimal design. The absorber consists of a pneumatic cylinder with a sleeve and a piston. The piston is equipped with a valve to control gas flow between the two chambers of the cylinder [32]. A horizontal configuration of the absorber is considered, typical for bumpers and production lines. Unlike in landing gear applications, this allows gravity to be neglected and thus makes the design process independent of aircraft- and mission-specific constraints and non-impact loads related to ground operations and particular values of the lift factor. First, a mathematical model of the absorber is presented along with the semi-active control method, and then a formal design procedure is developed. Given the required ranges of impact conditions and design parameters, the proposed formulation aims to minimize two practical criteria treated as objectives: (1) the maximum deceleration of the impacting object, and (2) the maximum gas flow rate the valve must provide to ensure effective control. As in many other optimization problems in engineering [33], these objectives are partially conflicting, which leads to a multi-objective optimization approach. The determined Pareto-optimal design parameters provide the desired trade-off

between the criteria and ensure the operational capacity of the absorber within the prescribed range of impacts.

This paper is structured as follows. Section 2 briefly discusses the concept of absorber efficiency, describes the specific absorber under consideration, introduces the impact and design parameters, and states the absorber design problem. Section 3 describes the mathematical model of the impact absorption process, the optimal semi-active control scheme, and the two employed objective functions. An example optimization is presented in Sec. 4. It involves separate optimizations for each objective functions, as well as a systematic joint optimization that yields Pareto-optimal designs. Finally, Subsec. 4.4 and the conclusion discuss the results, their limitations, and summarize the paper.

2. Problem statement

Subsection 2.1 discusses the fundamental notion of absorber efficiency and the optimal profile of its reaction force. Then, Subsec. 2.2 describes the considered absorber. This paper addresses the problem of determining the values of the selected design parameters (listed in Subsec. 2.5) that optimize the absorber's operational capacity for impacts within the range defined by the assumed impact parameters (Subsec. 2.3).

2.1. Absorber efficiency and maximum force

A fundamental concept in impact absorbers is absorber efficiency. It is defined as the ratio of the area enclosed between the force-displacement curves of the absorber's reaction forces $F_{\rightarrow}(x)$ and $F_{\leftarrow}(x)$ (corresponding, respectively, to the piston's forward motion caused by the decelerated object and to its return stroke, see Fig. 1) to the area of the smallest enclosing rectangle (the rectangle's

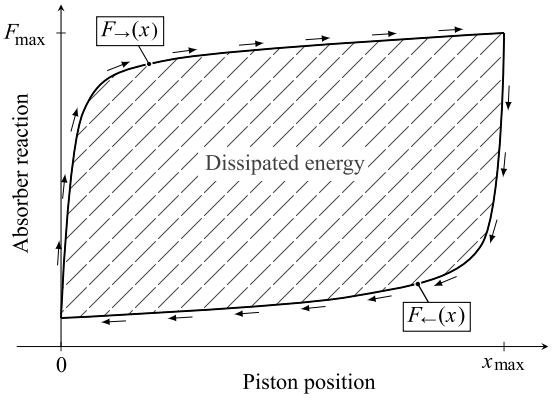

Fig. 1. Schematic representation of the work cycle of an impact energy absorber.

height is equal to the maximum reaction force $F_{\max}$ of the absorber, and the width corresponds to the total stroke length $x_{\max}$ of the piston) [7]:

$$\eta = \frac{1}{F_{\max}\, x_{\max}} \left(\int_0^{x_{\max}} F_{\rightarrow}(x)\, \mathrm{d}x - \int_0^{x_{\max}} F_{\leftarrow}(x)\, \mathrm{d}x \right), \tag{2.1}$$

where the coordinate x, as shown in Fig. 2, is measured from the extreme position of the piston $x = 0$, which corresponds to the maximum extension of the absorber in its initial position.

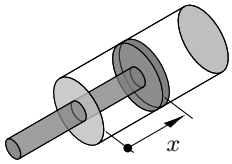

FIG. 2. Coordinate x of the piston position in the cylinder.

When designing an absorber and/or its control algorithm, maximization of the efficiency η can focus on the following three goals:

1) ensuring the flattest force profile $F_{\rightarrow}(x)$ while moving the piston from its initial position $x = 0$ to its final position $x_{\max}$ in the cylinder,
2) ensuring that the piston displacement $x_{\max}$ is as long as possible, and preferably equal to the entire available absorber stroke x_0,
3) reducing the return force $F_{\leftarrow}(x)$ to minimum.

The first two goals focus on the breaking force profile $F_{\rightarrow}(x)$ and aim at reducing the maximum force $F_{\max}$. They are fundamental for increasing absorber efficiency and can be addressed through proper control algorithms and valves that release gas from the compressed chamber to the other chamber, the surroundings, or a dedicated external container [34]. The third goal focuses on the return force $F_{\leftarrow}(x)$, and it is best achieved by using valves that release gas from the cylinder to the surroundings when the piston reaches its final position, which instantaneously releases the energy stored in the absorber and prevents the stopped object from being accelerated back by the retracting piston [35]. However, the released gas has to be pumped back before the next absorption cycle, which requires significant energy and contradicts the intended semi-active character of the absorber. Therefore, semi-active solutions for reusable impact absorbers focus usually on in-piston valves and internal gas flow between the cylinder chambers [27, 32].

2.2. The considered absorber

A schematic of the pneumatic absorber considered in this paper is depicted in Fig. 3. Its main components include a cylinder, a piston, and a piston rod. The piston is equipped with a valve that enables the control of gas flow between the two sealed chambers of the cylinder. This allows the reaction force of the piston rod to be controlled in real time during the impact absorption process. The instantaneous reaction force is determined based on the pressures inside the cylinder, obtained using two pressure transducers labeled as p_1 and p_2. The system controller, which calculates the reaction force and controls the valve, is a component of the feedback loop.

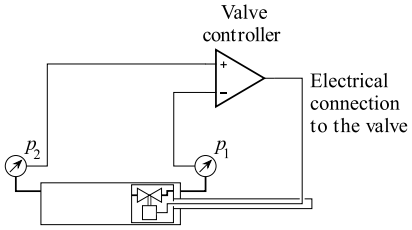

FIG. 3. Schematic of the considered pneumatic absorber.

As discussed in Subsec. 2.1, an advantage of this general design is that such an absorber can be used for repeated stopping of objects. There is no need to replenish the gas after each impact, and, due to various surface areas on the two sides of the piston, the pressure-related forces autonomously return the piston to its initial state upon opening the valve, which ensures readiness for the next operational cycle.

The controllability of the valve allows the absorber operation to be adjusted to different impact parameters (Subsec. 2.3): the piston can potentially move along the entire available stroke, and the reaction force profile can be made as flat as possible. Such a system is **adaptive** (it adjusts to operational conditions) [21] and **semi-active** (it does not require any significant external energy, other than that necessary to control the valve opening) [18].

2.3. Impact parameters

In this paper, the impact to be absorbed is assumed to be fully defined in terms of the two following parameters:

1) mass $M \in \mathcal{M}$ of the impacting object, and
2) velocity $v \in \mathcal{V}$ of the impacting object.

The symbols $\mathcal{M}$ and $\mathcal{V}$ denote the considered ranges of the impact parameters. The Cartesian product of $\mathcal{M}$ and $\mathcal{V}$ is denoted by $\mathcal{I} = \mathcal{M} \times \mathcal{V}$. This paper

focuses on absorber design, not on optimal control, and the specific values of these parameters are assumed to be known (or identified) before each impact, as required for the purpose of optimal control [36].

2.4. Objective functions and absorber design problem

This paper addresses the problem of optimal absorber design. It is formulated as a multi-objective optimization task of simultaneous minimization of: (1) the maximum deceleration of the impacting object, and (2) the maximum mass flow rate through the valve required for optimal control. This can be formalized as follows: given a set $\mathcal{I}$ of expected impact parameters $\mathbf{i} = (M, V) \in \mathcal{I}$, minimize:

1) the maximum deceleration $a_{\max}$ of the impacting object provided by the optimally controlled absorber, and
2) the mass flow rate f_R through the valve required for optimal control,

with respect to the design parameters $\mathbf{d} \in \mathcal{D}$ (defined in Subsec. 2.5):

$$\mathbf{d}_{\text{opt}} = \underset{\mathbf{d}\in\mathcal{D}}{\operatorname{argmin}} \begin{cases} \max_{\mathbf{i}\in\mathcal{I}} \ a_{\max}(\mathbf{i}, \mathbf{d}), \\ \max_{\mathbf{i}\in\mathcal{I}} \ f_R(\mathbf{i}, \mathbf{d}). \end{cases} \tag{2.2}$$

The term $a_{\max}(\mathbf{i}, \mathbf{d})$ denotes the maximum deceleration of the optimally controlled absorber, with such control described in Subsec. 3.2. Similarly, the term $f_R(\mathbf{i}, \mathbf{d})$ represents the minimum mass flow rate that ensures the optimal control of absorber $\mathbf{d}$ can actually be realized for impact $\mathbf{i}$. These two objective functions are described in detail in Subsec. 3.3.

Equation (2.2) defines a multicriterial optimization problem. As such, it is expected to yield multiple optimal (nondominated) solutions, which together form the Pareto front. Analyzing the Pareto front can provide insights into the attainable trade-offs between the two considered design criteria. The Pareto front can also be used to guide the selection of a specific valve product: first, an acceptable limit for deceleration can be determined, and then the corresponding required maximum mass flow rate can be read from the Pareto front.

2.5. Absorber design parameters

Given the initial velocity and the mass of the impacting object, the performance of an impact energy absorber depends on its design parameters. Among these, the most important are:

1) the maximum available piston stroke x_0, see Fig. 4a,
2) the piston active area on the compressed side A_2, see Fig. 4b, which is expressed in terms of the diameter ϕ_2 of the compressed chamber as $A_2 = \pi\phi_2^2/4$. The piston rod cross-sectional area ΔA is usually determined a priori, and the opposite-side piston active area is then $A_1 = A_2 - \Delta A$,

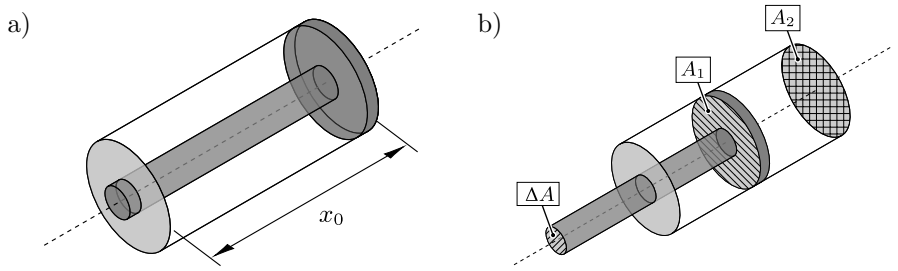

FIG. 4. Maximum available piston stroke x_0 (a), and surfaces subjected to gas pressure (b).

3) the initial pressure p_0 inside the pneumatic cylinder, assumed to be the same in both chambers,
4) the mass flow capacity of the piston valve, expressed here in units of g/s.

In this paper, the flow capacity of the piston valve is assumed to be sufficiently high for the purpose of optimal control, and it is treated as an objective function, as described in Subsec. 2.4. Thus, only the first three of the above parameters can be adjusted, which yields three design parameters to be considered in the design procedure: stroke length x_0, diameter of the compressed chamber ϕ_2, and initial pressure p_0. Consequently, the design variable is the three-element vector $\mathbf{d} = (x_0, \phi_2, p_0)$, and the Cartesian product of the intervals of their allowable values constitutes the design space $\mathcal{D}$.

3. Mathematical models of the absorption process and optimum control

This section describes the formal model of the absorption process (Subsec. 3.1) and the optimal control procedure (Subsec. 3.2). Thereupon, the two objective functions used in the proposed optimal design procedure are introduced (Subsec. 3.3). The symbols used in this section are illustrated in Fig. 5.

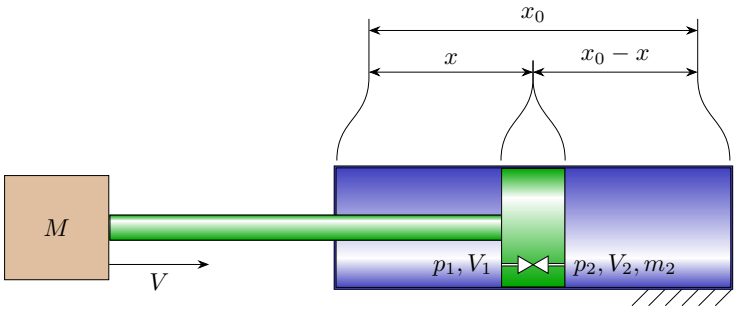

FIG. 5. Schematic view of the absorber with the impacting mass and symbols used in this paper.

3.1. Model of the absorption process

3.1.1. Forward movement of the piston. The forward movement is the crucial phase of the impact absorption process. It can be described in terms of the three state variables: $x(t)$, $p_1(t)$, and $p_2(t)$ by the following equation:

$$M\ddot{x}(t) = -F(t) = A_1 p_1(t) - A_2 p_2(t), \tag{3.1}$$

which is the equation of motion of the impacting object, whose acceleration is proportional to the reaction force (or the difference of forces acting on the two sides of the piston). The mass of the piston itself is assumed to be much smaller than that of the impacting object and is thus neglected:

$$\frac{p_2(t)V_2^{\kappa}(t)}{m_2^{\kappa}(t)} = \frac{p_2(0)V_2^{\kappa}(0)}{m_2^{\kappa}(0)} = \text{const} \tag{3.2}$$

is the mass-normalized polytropic equation for the second (compressed) chamber. It is valid during the forward motion of the piston, as long as there is no reverse flow of the gas through the valve, that is, at least until $x = x_{\max}$ is reached. The impact process is assumed to be fast, and consequently, there is no heat exchange with the surroundings, and $\kappa = 1.4$. Finally,

$$\frac{1}{2}MV^2 - \frac{1}{2}M\dot{x}^2(t) = \frac{p_1(t)V_1(t) + p_2(t)V_2(t) - p_2(0)V_2(0)}{\kappa - 1} \tag{3.3}$$

describes the energy balance for the entire system: the decrease in the kinetic energy of the impacting object, which equals the change in the internal energy of the gas in both chambers. The initial volume of the first chamber, that is, the clearance volume $V_1(0)$, is assumed to be zero, so it does not appear in Eq. (3.3).

Equations (3.1)–(3.3) are complemented with the following initial conditions and relations:

$$\begin{aligned} x(0) &= 0, & p_1(0) &= p_0, \\ \dot{x}(0) &= V, & p_2(0) &= p_0, \\ V_1(t) &= A_1 x(t), & m_2(0) &= p_0 V_2(0)/RT, \\ V_2(t) &= A_2\left(x_0 - x(t)\right), & \kappa &= 1.4, \end{aligned} \tag{3.4}$$

where R is the specific gas constant and T is the ambient temperature. To account for pressure equalization due to valve opening during the return movement of the piston, it is assumed that $p_1(0) = p_2(0)$. However, since the clearance volume $V_1(0)$ is zero, the specific initial value $p_1(0)$ does not affect the absorption process.

3.1.2. Reverse movement of the piston. As discussed in Subsec. 2.2, the reverse movement of the piston is ensured by pressure-related forces due to the various surface areas on the two sides of the piston, and reverse motion happens autonomously upon valve opening. This movement is secondary for the design of the absorber and is not considered further.

3.1.3. Control function. The variable $m_2(t)$ in Eq. (3.2) denotes the mass of gas in the compressed chamber. Its derivative $\dot{m}_2(t)$ is the mass flow rate through the valve, which is instantaneously and directly related to the opening of the valve. The specific form of this relationship depends on the technical characteristics of particular valves used, and therefore $\dot{m}_2(t)$ is treated here as a general surrogate control function governing the process.

3.2. Optimum control

3.2.1. Instantaneously constant reaction force. During the forward movement of the piston, as long as the pressure difference between the chambers is positive, $p_2(t) > p_1(t)$, there is a control function $\dot{m}_2(t)$ that maintains the reaction force at its current level, so that $\dot{F}(t) = 0$. This control can be determined as follows. The reaction force F is expressed by Eq. (3.1). If it remains constant, its time derivative must vanish:

$$\dot{F}(t) = A_2\dot{p}_2(t) - A_1\dot{p}_1(t) = 0. \tag{3.5}$$

Substituting of Eqs. (3.1) and (3.5) into the differentiated Eq. (3.2) yields:

$$\dot{p}_2(t) = \frac{\kappa F(t)\dot{x}(t)}{V_2(0)}. \tag{3.6}$$

This, when substituted into the differentiated Eq. (3.2), which is:

$$\dot{p}_2(t) = \kappa p_2(t)\left(\frac{\dot{m}_2(t)}{m_2(t)} - \frac{\dot{V}_2(t)}{V_2(t)}\right), \tag{3.7}$$

yields the following formula:

$$\frac{\dot{m}_2(t)}{m_2(t)} = \frac{F(t)\dot{x}(t)}{p_2(t)V_2(0)} + \frac{\dot{V}_2(t)}{V_2(t)}. \tag{3.8}$$

Given Eqs. (3.2) and (3.4), the intended control $\dot{m}_2(t)$ is expressed in Eq. (3.8) in terms of directly measurable quantities.

3.2.2. Maximum and minimum reaction forces. All reaction forces achieved during the forward movement of the piston must lie between the two extreme values:

– the maximum force $f_{\max}(x_F)$, which is attained when the valve is kept completely closed for the entire stroke from 0 to x_F:

$$f_{\max}(x_F) = p_0 A_2 \left(\frac{x_0}{x_0 - x_F} \right)^{\kappa}; \tag{3.9}$$

– the minimum force $f_{\min}(x_F)$, which is attained if the flow through the valve is high enough to equalize the chamber pressures before the full stroke x_0 is reached. This force equals the product of the common pressure, $p_1 = p_2$, and the piston rod cross-section area ΔA. However, this common, equalized pressure depends on the energy already absorbed during the stroke from 0 to x_F. Assuming the intended flat reaction force profile:

$$F(x) = \text{const} = f_{\min}(x_F) \qquad \text{for} \qquad x \in [0, x_F], \tag{3.10}$$

the minimum force $f_{\min}(x_F)$ can be determined by solving the following system of equations:

$$p_1(x_F) = p_2(x_F), \tag{3.11}$$

$$f_{\min}(x_F) = A_2 p_2(x_F) - A_1 p_1(x_F), \tag{3.12}$$

$$x_F f_{\min}(x_F) = \frac{p_1(x_F)V_1(x_F) + p_2(x_F)V_2(x_F) - p_0 V_2(0)}{\kappa - 1}, \tag{3.13}$$

where the last two equations correspond to Eqs. (3.1) and (3.3), and $x_F f_{\min}(x_F)$ represents the energy already absorbed. Taking into account Eq. (3.4), the solution is:

$$f_{\min}(x_F) = p_0 \Delta A \left(1 - \kappa \frac{x_F}{x_0} \frac{\Delta A}{A_2} \right)^{-1}, \tag{3.14}$$

$$p_1(x_F) = p_2(x_F) = \frac{f_{\min}(x_F)}{\Delta A}. \tag{3.15}$$

The minimum and maximum forces defined in Eqs. (3.14) and (3.9) are illustrated in Fig. 6. Due to the different magnitudes of $f_{\min}(x_F)$ and $f_{\max}(x_F)$, the vertical axis is shown on a logarithmic scale.

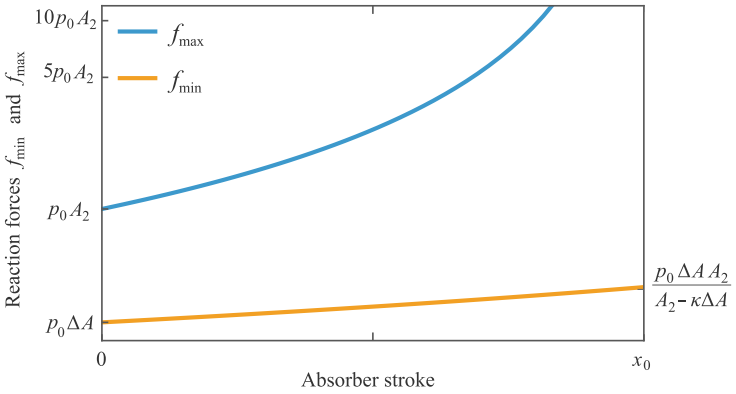

FIG. 6. Minimum and maximum reaction forces as a function of the absorber stroke. The vertical axis is shown on logarithmic scale.

3.2.3. Optimal reaction force profile. In line with Subsec. 2.1, the optimal control minimizes the maximum deceleration, $a_{\max} = -\ddot{x}_{\min}$, occurring during the braking process. For each specific impact parameter M, since $F(t) = -\ddot{x}(t)/M$, this is equivalent to minimizing the maximum reaction force. As discussed in Subsec. 2.4, such a control goal can be achieved by maintaining a flat reaction force profile over a possibly long stroke, preferably the entire available length of x_0. Taking into account the upper and lower force bounds, $f_{\max}$ and $f_{\min}$, this yields three optimal force profiles and control schemes, depending on the initial kinetic energy E of the impact. These are illustrated in Fig. 7 and defined as follows:

1) *High impact energy*: $E \geq x_0 f_{\max}(0)$. The optimal reaction force initially follows the upper bound $f_{\max}(x)$. Then, upon achieving the optimal level F_{opt},

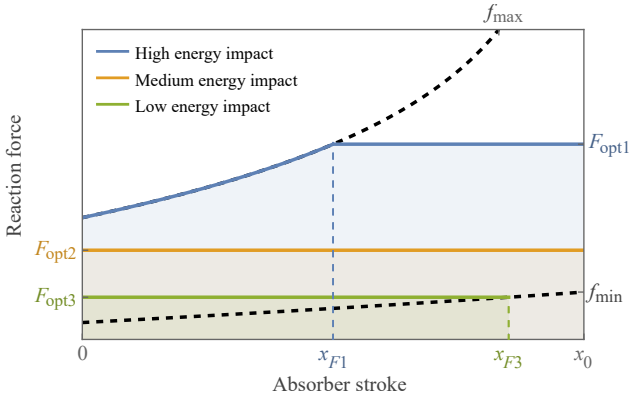

FIG. 7. Optimal reaction force profiles as a function of the absorber stroke for three levels of impact energy. The colored regions represent the absorbed energies. The vertical axis is shown on logarithmic scale.

it remains constant till the end of the full absorber stroke x_0. The optimal force F_{opt} can be related to the impact energy E by requiring that E is fully absorbed over the entire stroke of x_0:

$$E = \int_0^{x_F} f_{\max}(x)\,\mathrm{d}x + (x_0 - x_F)F_{\text{opt}} = \frac{A_2 p_0 x_0}{\kappa - 1}\left(\kappa\left(\frac{x_0}{x_0 - x_F}\right)^{\kappa-1} - 1\right), \tag{3.16}$$

where $x_F = f_{\max}^{-1}(F_{\text{opt}})$ is the stroke at which the optimal force F_{opt} is achieved.

2) *Medium impact energy*: $x_0 f_{\min}(x_0) \le E < x_0 f_{\max}(0)$. The optimal reaction force profile is flat over the entire piston stroke from 0 till x_0. The optimal reaction force F_{opt} is related to the impact energy E as:

$$E = x_0 F_{\text{opt}}. \tag{3.17}$$

3) *Low impact energy*: $E < x_0 f_{\min}(x_0)$. The optimal force profile is flat, but the stroke extends only till $f_{\min}$ is reached, and the pressure in both chambers is equalized before x_0 is attained. The optimal reaction force F_{opt} is related to E as:

$$E = x_F\, f_{\min}(x_F) = x_F F_{\text{opt}}, \tag{3.18}$$

where $x_F = f_{\min}^{-1}(F_{\text{opt}})$ is the stroke at which pressures in both chambers become equal, see Eq. (3.11), and $f_{\min}$ is reached.

Equations (3.16)–(3.18) link the optimal reaction force F_{opt} to the impact energy E in an implicit manner. When resolved analytically and collected together, they yield:

$$F_{\text{opt}}(E) = \begin{cases} A_2 p_0\left(\dfrac{1}{\kappa} + \dfrac{\kappa - 1}{\kappa}\dfrac{E}{A_2 p_0 x_0}\right)^{\frac{\kappa}{\kappa-1}} & \text{if } E \in [x_0 f_{\max}(0), \infty), \\ E/x_0 & \text{if } E \in [x_0 f_{\min}(x_0), x_0 f_{\max}(0)), \\ \Delta A\left(p_0 + \dfrac{\kappa E}{A_2 x_0}\right) & \text{if } E \in (0, x_0 f_{\min}(x_0)). \end{cases} \tag{3.19}$$

3.3. Objective functions

3.3.1. Maximum deceleration. The first of the two objective functions considered in Subsec. 2.3 is the maximum deceleration:

$$a_{\max} = -\ddot{x}_{\min} = -\min_t \ddot{x}(t). \tag{3.20}$$

For an optimally controlled absorber, the maximum reaction force equals F_{opt}, and thus the maximum deceleration is the following function of the impact parameters:

$$a_{\max}(M,V) = \frac{F_{\text{opt}}\left(\frac{1}{2}MV^2\right)}{M}, \tag{3.21}$$

where M and V represent the mass and velocity of the impacting object, respectively see Subsec. 2.3.

3.3.2. Mass flow rate. The second objective function considered in Subsec. 2.4 is the minimum mass flow rate through the valve that ensures the optimal control is technically feasible. It equals the maximum flow rate attained during the absorption process:

$$f_R = -\min_t \dot{m}_2(t), \tag{3.22}$$

and it can be computed analytically as described further.

First, the mass m_2 is analytically expressed in terms of the piston displacement x. To this end, Eq. (3.2) is used to express m_2 during the control phase (that is, when the reaction force equals F_{opt}) in terms of the pressure $p_2(x)$:

$$m_2(x) = m_2(0)\left(\frac{p_2(x)}{p_2(0)}\right)^{\frac{1}{\kappa}} \frac{V_2(x)}{V_2(0)}, \tag{3.23}$$

where the pressure $p_2(x)$ is determined, along with $p_1(x)$, by solving the following system of two linear equations:

$$F_{\text{opt}}(E) = A_2 p_2(x) - A_1 p_1(x), \tag{3.24}$$

$$E_{\text{absorbed}}(x) = \frac{p_1(x)V_1(x) + p_2(x)V_2(x) - p_0V_2(0)}{\kappa - 1}, \tag{3.25}$$

which correspond to Eqs. (3.1) and (3.3). The symbol $E_{\text{absorbed}}(x)$ denotes the kinetic energy already absorbed during the forward movement of the piston up to x. Given the constant reaction force in the optimally controlled absorber, it can be expressed as:

$$E_{\text{absorbed}}(x) = \begin{cases} E - (x_0 - x)F_{\text{opt}} & \text{if } E \in [x_0 f_{\max}(0), \infty), \\ xF_{\text{opt}} & \text{if } E \in (0, x_0 f_{\max}(0)). \end{cases} \tag{3.26}$$

Then, given $m_2(x)$, the mass flow rate $\dot{m}_2$ is expressed analytically in terms of the piston displacement x:

$$\dot{m}_2(x) = \frac{\mathrm{d}}{\mathrm{d}t} m_2(x(t)) = \frac{\mathrm{d}m_2(x)}{\mathrm{d}x}\frac{\mathrm{d}x}{\mathrm{d}t} = m_2'(x)\,\dot{x}, \tag{3.27}$$

where the velocity $\dot{x}$ can be expressed in terms of the piston displacement x based on the current kinetic energy of the mass M:

$$\frac{1}{2}M\dot{x}^2(x) = E - E_{\text{absorbed}}(x). \tag{3.28}$$

Finally, given $\dot{m}_2(x)$, its derivative with respect to x is computed and set equal to zero. The solutions of the resulting equation, together with the strokes at both ends of the flat-force profile, are the candidate piston strokes at which the maximum mass flow rate f_R can be attained. Using the already derived analytical formula for $\dot{m}_2(x)$, the corresponding mass flow rates can be computed and compared to determine the actually required mass flow rate f_R.

4. Example of design optimization

4.1. Impact and design parameters

The considered impact scenarios involve impacting masses ranging from 1 kg to 11 kg, $M \in [1, 11]$ kg. These scenarios could represent potential applications, which may include 1 kg transporter cart or packaging with up to 10 kg actual mass. The range of impact velocities V is $[0, 5]$ m/s. These values may correspond to typical small-item handling scenarios in factory settings. The considered design domain $\mathcal{D}$ is defined by the following ranges of the three design parameters:

- absorber length $x_0 \in [100, 200]$ mm,
- initial pressure $p_0 \in [2, 10]$ atm,
- diameter of the compressed chamber $\phi_2 \in [25, 40]$ mm, which corresponds to the area $A_2 \in [491, 1257]$ mm^2.

These ranges correspond to typical lab-sized absorbers, which may facilitate further experimental testing. The design and impact parameters, as well as other important technical parameters of the absorber, are listed in Table 1.

Table 1. Ranges and values of parameters used in Sec. 4.

Symbol	Value	Description
M	$[1, 11]$ kg	Mass of the impacting object
V	$[0, 5]$ m/s	Velocity of the impacting object
x_0	$[100, 200]$ mm	Absorber length
p_0	$[2, 10]$ atm	Initial pressure
ϕ_2	$[25, 40]$ mm	Diameter of the compressed chamber
A_2	$[491.9, 1257]$ mm^2	Piston area on the compressed side, $A_2 = \pi\phi_2^2/4$
ΔA	113.1 mm^2	Piston rod cross-sectional area (diameter 12 mm)
T	293.15 K	Initial gas temperature (20°C)
R	296.8 J/(kg · K)	Specific gas constant for nitrogen

4.2. Individual objective functions

Subsection 2.4 defines the absorber design problem in terms of two objective functions. In this Subsec. 4.2, these two objective functions are considered separately. Their joint (multi-objective) minimization is considered in the subsequent Subsec. 4.3.

4.2.1. Maximum deceleration. Figure 8 presents the isosurfaces of the first objective function within the design domain. Its dependence on the design variables can be summarized as follows:

- the dependence on the absorber length x_0 is clear and intuitive: the longer the absorber, the longer the braking distance, and, consequently, the lower the deceleration,
- similarly, the larger the piston diameter ϕ_2, the greater the force that can be instantaneously generated in the high-energy impact scenario (at the beginning of the stroke, see Eq. (3.9)), and the lower the resulting optimal force level and deceleration. In low-energy scenarios, increasing the diameter ϕ_2 decreases the minimum force $f_{\max}$ and, consequently, the deceleration, see Eq. $(3.19)_3$,
- the dependence on the initial pressure p_0 is more complex. On one hand, higher pressure shortens the braking distance in low-energy impact scenarios, which causes small masses to experience higher decelerations. On the other hand, in high-energy impact scenarios, lower pressure prolongs

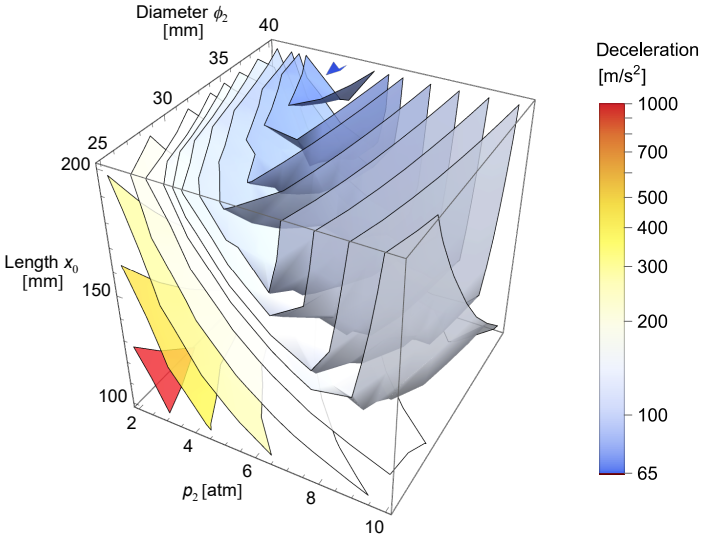

FIG. 8. Isosurfaces of the maximum deceleration of the impacting object, $\max_{\mathbf{i}} a_{\max}(\mathbf{d})$, within the design domain.

the initial force buildup phase along $f_{\max}$, and, as a result, the optimal flat reaction force is higher, so large masses experience higher decelerations. Such a dependence on impact masses and pressures suggests that the minimum is attained when the decelerations of the largest and smallest masses (at the maximum impact velocity) are equal. Based on Eq. (3.19), this yields the following equation for the optimal $\widetilde{p}_0$, which has to be solved numerically:

$$\frac{A_2 p_0}{M_{\max}} \left(\frac{1}{\kappa} + \frac{\kappa - 1}{\kappa} \frac{M_{\max} V_{\max}^2}{2 A_2 \widetilde{p}_0 x_0} \right)^{\frac{\kappa}{\kappa - 1}} = \frac{\Delta A}{M_{\min}} \left(\widetilde{p}_0 + \kappa \frac{M_{\min} V_{\max}^2}{2 A_2 x_0} \right). \tag{4.1}$$

It can be noted that the optimal reaction force F_{opt} in high-energy impacts depends only on the product $A_2 p_0$ and not independently on p_0 and A_2, see Eq. (3.19). This reduces the effective number of design parameters, so that, for a given absorber length x_0, the isolines of both objective functions are parallel.

The global minimum within the design domain is attained for $x_0 = 200$ mm, $p_0 = 4.795$ atm, and $\phi_2 = 40$ mm. This worst-case deceleration is equal to 62.82 m/s^2. It is relatively close to the value of 62.5 m/s^2 that would be attained with a constant reaction force over the entire piston stroke in the mid-energy impact scenario.

4.2.2. Mass flow rate. The isosurfaces of the second objective function are shown in Fig. 9. The dependence on the absorber length x_0 is similar to that of

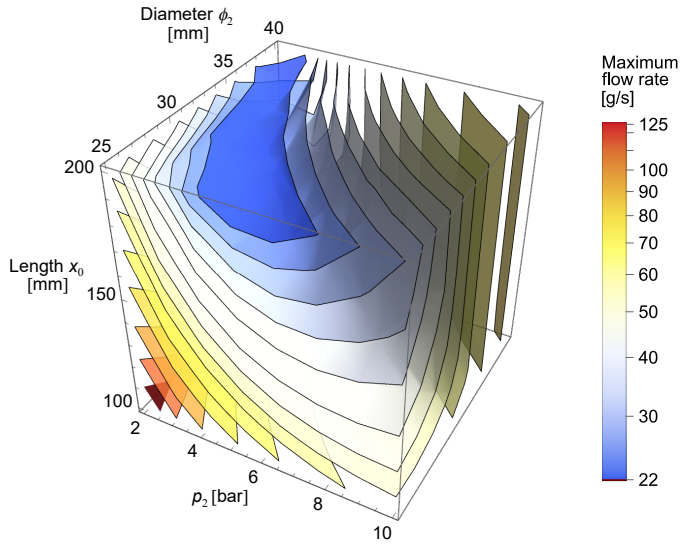

FIG. 9. Isosurfaces of the maximum flow rate $\max_{\mathbf{i}} f_R(\mathbf{d})$ achieved during the absorption process.

the first objective function: the longer the absorber, the smaller the maximum flow rate that the valve must provide. The dependence on the initial pressure p_0 and the diameter ϕ_2 is more complex. With the absorber length fixed, the minimum is attained for the largest impact mass and velocity. It lies along a curved line defined by $p_0 V_2 = \text{const}$ and is not unique. The global minimum is 20.89 g/s, achieved for $x_0 = 200$ mm. The corresponding optimal pressures and diameters, (p_0, ϕ_2), extend along a curved line from (5.866 atm, 25 mm) to (2.291 atm, 40 mm).

4.3. Multi-objective optimization

Both objective functions have the same straightforward dependence on the absorber length x_0 (the longer the absorber, the better the outcome). This suggests that x_0 can be treated as an independent design parameter. The multi-objective optimization should then be performed with respect to the pressure p_0 and the diameter ϕ_2, independently for each selected absorber length x_0.

Figure 10 shows the Pareto fronts in the objective function space, computed for several absorber lengths. These fronts reveal the optimal designs attainable for the indicated length x_0 within the considered ranges of p_0 and ϕ_2. Their L-like shapes illustrate the best trade-offs between the two design criteria.

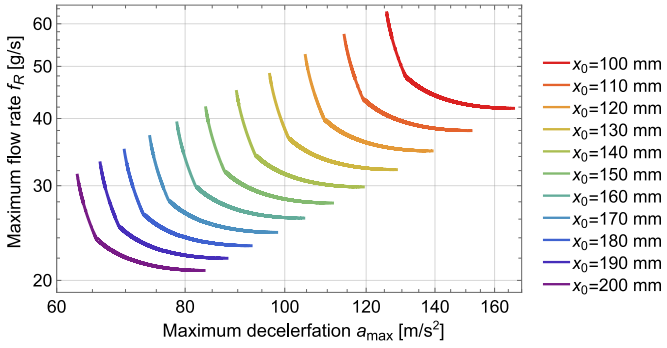

FIG. 10. Pareto fronts in the space of objective functions, computed for various absorber lengths x_0.

Pareto fronts in the design space, computed for $x_0 = 100$ mm and 200 mm, are shown in the bottom row of Fig. 11. Their shape is atypical: due to the partially parallel isolines of the objective functions, they locally become Pareto regions. The top row shows these fronts in the objective function space. The top and bottom row Pareto fronts are connected by colors: their corresponding points share the same color. This coloring scheme allows for easy identification, in the bottom plots, of the absorber designs corresponding to different sections of the top-plot Pareto fronts. In other words, each color represents a pair of

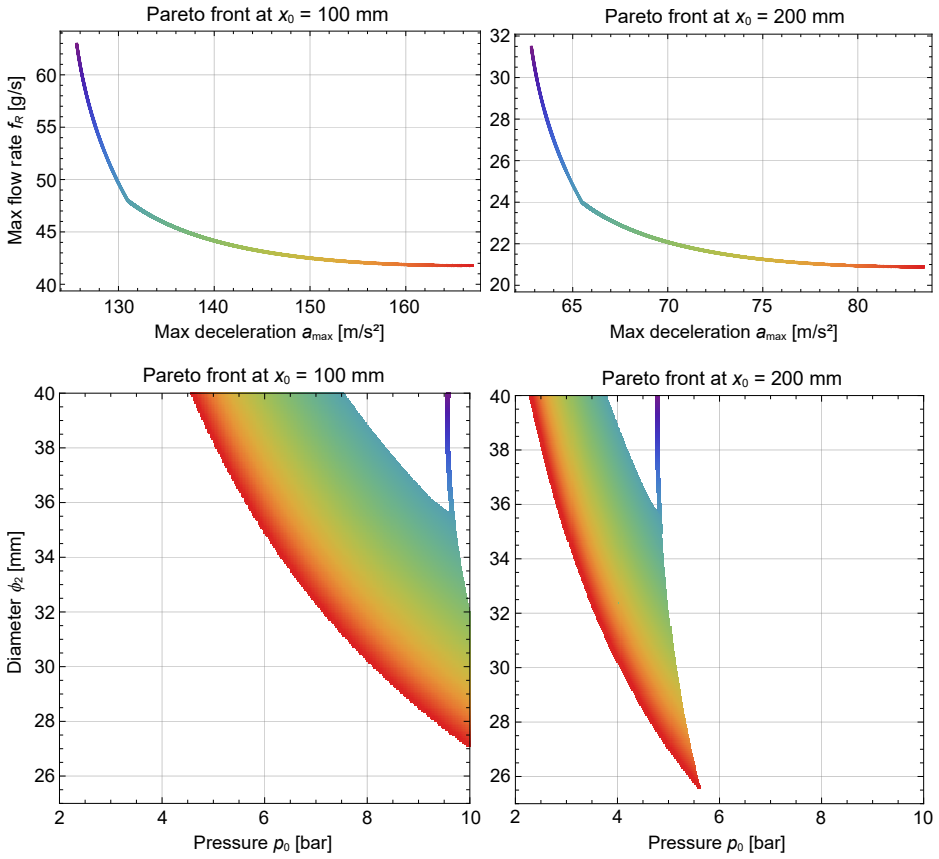

FIG. 11. Pareto fronts in the space of objective functions (top row) and the design space (bottom row), computed for $x_0 = 100$ mm and 200 mm. The bottom plots are color-coded according to the corresponding points in the top plots, which serve as a form of 2D legends for the bottom plots.

objective function values, and the top-plot Pareto fronts serve as a form of 2D legends for the bottom plots.

4.4. Discussion

4.4.1. Shape of the Pareto fronts. In the lower-pressure region of the design space, the isolines of both objective functions are mutually parallel. This region corresponds to the maximum deceleration and maximum flow rate achieved with the highest possible impact energy E (maximum velocity V and maximum mass M), where such an impact falls within the mid- and high-energy impact scenarios of the absorbers. In this region, the isolines of both objective functions are defined by the equation $p_0 V_2(0) = \text{const}$, and, therefore, are parallel.

This reduces the effective number of design variables and locally transforms the Pareto fronts in the design space into Pareto regions.

Conversely, in the higher-pressure region of the design space, the maximum deceleration and maximum flow rate occur in low-impact energy scenarios (high impact velocity but low mass). In these scenarios, the maximum absorber stroke – and thus the entire dynamics of the process – depends on the pressure p_0 independently of the product $p_0V_2(0)$. This decouples the design variables of p_0 and ϕ_2: the isolines of the objective functions are thus no longer parallel, and the Pareto fronts take on their typical one-dimensional form of lines.

4.4.2. Pareto-optimal solutions. Analyzing the Pareto fronts in the design space (bottom row in Fig. 11) can help in selecting a design that ensures an appropriate trade-off between the two objective functions. For each given absorber length, their individual minima lie in the design space relatively close to each other. It is thus natural to assume that the optimal solutions lie between these two minima. However, an analysis of the Pareto fronts in Fig. 11 (bottom row) reveals that certain regions near the individual minima are non-optimal and should be avoided.

4.4.3. Design flexibility. Finally, the results reveal that relatively large portions of the design space belong to the Pareto front and are Pareto-optimal. In particular, if minimizing the maximum deceleration $a_{\max}$ is the highest priority, there is only a single Pareto-optimal point in the design space, represented by the purple end of the fronts shown in Fig. 11 (bottom row). However, if the constraint on maximum deceleration is slightly relaxed – or equivalently, if a longer absorber is allowed – the Pareto-optimal points shift toward the opposite red end of the respective fronts and cover increasingly larger regions of the design space. This increases flexibility of the optimal design process and facilitates the incorporation of additional secondary objective functions without affecting the primary performance.

5. Conclusion

This manuscript proposes a formal multi-objective design process for an adaptive pneumatic impact absorber. A horizontal absorber configuration (as used in bumpers or production lines) is considered focusing on impact-related effects while neglecting application-specific effects that arise from non-impact operational loads and gravity. The absorber consists of two sealed chambers, separated by a piston equipped with a controllable valve. Proper valve control can ensure a nearly flat profile of the reaction force. The design of

such a semi-actively controlled absorber is assumed to be defined by three parameters: absorber length, absorber diameter, and initial gas pressure. A range of impact scenarios is considered, defined in terms of impacting mass and velocity. Two objective functions are defined (the maximum deceleration of the impacting object and the maximum gas flow rate through the valve), which yields a multi-objective optimization problem. Proper solution of this problem yields formally optimal trade-offs between the two objectives and makes the design process more flexible.

Further work can address the limitations of the presented approach, such as the assumption of ideal valve dynamics (no gas leaks and no control delays), neglected friction, or the robustness of the design to control disturbances. A secondary degree of freedom could also be introduced to account for the interface between the piston and the impacting mass (such as a rubber bumper). Additionally, vertical configurations of the absorber (as in landing gear applications) could be considered. This would require gravity and the lift factor to be incorporated into the governing equations and would introduce additional constraints related to post-landing ground operations and non-impact operational loads.

Acknowledgments

The second author (C.G.) acknowledges the support of the National Science Centre, Poland, granted through the agreement 2018/31/D/ST8/03178.

Declaration of conflicting interest

The Authors declare that there are no known competing financial interests or personal relationships that could influence the work reported in this paper.

References

1. Holnicki-Szulc J., Graczykowski C., Mikułowski G., Mróz A., Pawłowski P., Wiszowaty R., Adaptive impact absorption – The concept and potential applications, *International Journal of Protective Structures*, **6**(2): 357–377, 2015, https://doi.org/10.1260/2041-4196.6.2.357.

2. Milecki A., Hauke M., Application of magnetorheological fluid in industrial shock absorbers, *Mechanical Systems and Signal Processing*, **28**: 528–541, 2012, https://doi.org/10.1016/j.ymssp.2011.11.008.

3. Willich F., Vrabec J., Holzapfel F., Single action control for oleo-pneumatic shock absorbers in CS-23 aircraft, *Aerospace Science and Technology*, **161**: 110078, 2025, https://doi.org/10.1016/j.ast.2025.110078.

4. Kęcik K., Simultaneous vibration mitigation and energy harvesting from a pendulum-type absorber, *Communications in Nonlinear Science and Numerical Simulation*, **92**: 105479, 2021, https://doi.org/10.1016/j.cnsns.2020.105479.

5. Graczykowski C., Mathematical models and numerical methods for the simulation of adaptive inflatable structures for impact absorption, *Computers and Structures*, **174**: 3–20, 2016, https://doi.org/10.1016/j.compstruc.2015.06.017.

6. Mikułowski G., Wiszowaty R., Holnicki-Szulc J., Characterization of a piezoelectric valve for an adaptive pneumatic shock absorber, *Smart Materials & Structures*, **22**(12): 1–12, 2013, https://doi.org/10.1088/0964-1726/22/12/125011.

7. Currey N.S., *Aircraft Landing Gear Design: Principles and Practices*, American Institute of Aeronautics and Astronautics, Washington, 1988.

8. Jurczyński M., Olszewski M., Methods of discrete pneumatic drive control that ensures the shock absorption during the last part of the movement, *Pomiary Automatyka Kontrola*, **55**(3): 209–212, 2009.

9. Bajkowski J.M., Bajer C.I., Dyniewicz B., Leonowicz M., Performance of a vibration damper using a new compressible magnetorheological fluid with microspheres, *Smart Materials and Structures*, **34**(1): 015041, 2025, https://doi.org/10.1088/1361-665X/ad9cd7.

10. Knap L., Makowski M., Siczek K., Kubiak P., Mrowicki A., Hydraulic vehicle damper controlled by piezoelectric valve, *Sensors*, **23**(4): 2007, 2023, https://doi.org/10.3390/s23042007.

11. Makowski M., Knap L., Study of a controlled piezoelectric damper, *Sensors*, **21**(10): 3509, 2021, https://doi.org/10.3390/s21103509.

12. Batterbee D.C., Sims N.D., Stanway R., Wołejsza Z., Magnetorheological landing gear: 1. A design methodology, *Smart Materials and Structures*, **16**(6): 2429–2440, 2007, https://doi.org/10.1088/0964-1726/16/6/046.

13. Moerman F., Dewulf S., Hygiene control in the application of compressed air and food gases, [in:] *Hygiene in Food Processing*, Lelieveld H.L.M., Holah J.T., Napper D. [Eds.], 2nd ed., pp. 203–255, Woodhead Publishing, 2014, https://doi.org/10.1533/9780857098634.2.203.

14. Stoll K., Halama H., *Pneumatic shock absorber*, US Patent 5,069,317, 12/1991.

15. Aginex, Oil-free air [in Polish: Powietrze bezolejowe], *Pneumatyka*, **82**(1): 7–11, 2012.

16. Rochowicz M., Developing systems with technical cleanliness requirements – constraints and new approaches, [in:] *23. Internationales Stuttgarter Symposium*, Kulzer A.C., Reuss H.C., Wagner A. [Eds], pp. 111–122, Springer Fachmedien, Wiesbaden, 2023, https://doi.org/10.1007/978-3-658-42236-3_9.

17. Chai S.T., Mason W.H., *Landing gear integration in aircraft conceptual design*, Technical Report MAD 96-09-01, Virginia Polytechnic Institute and State University, Blacksburg, 1997.

18. Pons J.L., *Emerging Actuator Technologies: A Micromechatronic Approach*, John Wiley & Sons, Chichester, 2005.

19. Niculescu A.I., *VZN. A New Damper Concept*, BREN, Bucharest, 2010.

20. Makowski M., Zalewski R., Vibration analysis for vehicle with vacuum packed particles suspension, *Journal of Theoretical and Applied Mechanics*, **53**(1): 109–117, 2015, https://doi.org/10.15632/jtam-pl.53.1.109.

21. Krüger W., *Integrated design process for the development of semi-active landing gears for transport aircraft*, PhD thesis, Institute of Flight Mechanics and Flight Control, University of Stuttgart, Hannover, 2000.

22. Wang H., Xing J.T., Price W.G., Li W., An investigation of an active landing gear system to reduce aircraft vibrations caused by landing impacts and runway excitations, *Journal of Sound and Vibration*, **317**(1): 50–66, 2008, https://doi.org/10.1016/j.jsv.2008.03.016.

23. McGehee J.R., Morris D.L., Active control landing gear for ground load alleviation, [in:] *AGARD Conference Proceedings*, FMP Symposium, Toronto, 1984.

24. Mikułowski G.M., *Adaptive impact absorbers based on magnetorheological fluids*, PhD thesis, Institute of Fundamental Technological Research, Polish Academy of Sciences, Warsaw, 2008.

25. Jiang P., Wang L., Yang T., Yang Z., Deep learning assisted semi-active control of magnetorheological buffer landing gear, [in:] *Proceedings of the International Congress on Sound and Vibration (ICSV 2024)*, van Keulen W., Kok J. [Eds], no. 202655, Society of Acoustics, Amsterdam, 2024.

26. Le Q.N., Park H.M., Kim Y., Pham H.H., Hwang J.H., Luong Q.V., An intelligent control and a model predictive control for a single landing gear equipped with a magnetorheological damper, *Aerospace*, **10**(11): 951, 2023, https://doi.org/10.3390/aerospace10110951.

27. Graczykowski C., *Inflatable structures for adaptive impact absorption*, PhD thesis, Institute of Fundamental Technological Research, Polish Academy of Sciences, Warsaw, 2012.

28. Faraj R., Mikułowski G., Wiszowaty R., Study on the state-dependent path-tracking for smart pneumatic shock-absorber, *Smart Materials and Structures*, **29**(11): 115008, 2020, https://doi.org/10.1088/1361-665X/ab9adc.

29. Graczykowski C., Faraj R., Extended identification-based predictive control for adaptive impact mitigation, *Bulletin of the Polish Academy of Sciences Technical Sciences*, **71**(4): e145937, 2023, https://doi.org/10.24425/bpasts.2023.145937.

30. Graczykowski C., Faraj R., Adaptive impact mitigation based on predictive control with equivalent mass identification, *Sensors*, **23**(3): 9471, 2023, https://doi.org/10.3390/s23239471.

31. Faraj R., Popławski B., Gabryel D., Mikułowski G., Wiszowaty R., On optimization of an adaptive pneumatic impact absorber – The innovative rescue cushion, *Bulletin of the Polish Academy of Sciences Technical Sciences*, **73**(3): e153436, 2025, https://doi.org/10.24425/bpasts.2025.153436.

32. Wiszowaty R., *Design and testing of adaptive pneumatic impact energy absorbers* [in Polish: *Projektowanie i badanie adaptacyjnych pneumatycznych absorberów energii uderzenia*], PhD thesis, Institute of Fundamental Technological Research, Polish Academy of Sciences, Warsaw, 2016.

33. Kęcik K., Brzeski P., Perlikowski P., Non-linear dynamics and optimization of a harvester-absorber system, *International Journal of Structural Stability and Dynamics*, **17**(5): 1740001, 2017, https://doi.org/10.1142/S0219455417400016.

34. Matsuhashi A., *Shock absorber*, US Patent 6,547,045, B2, 04/2003.

35. Antonovsky Y., *High frequency shock absorber and accelerator*, US Patent 6,454,061, B1, 09/2002.

36. Sekuła K., Graczykowski C., Holnicki-Szulc J., On-line impact load identification, *Shock and Vibration*, **20**(1): 147908, 2013, https://doi.org/10.3233/SAV-2012-0732.

Received March 28, 2025; accepted version May 16, 2025.
Online first October 2, 2025.